Random walks of colloidal probes in viscoelastic materials

Manas Khan and Thomas G. Mason*
Department of Physics and Astronomy and Department of Chemistry and Biochemistry, University of California-Los Angeles, Los Angeles, California 90095, USA
(Received 1 March 2014; published 29 April 2014)

To overcome limitations of using a single fixed time step in random walk simulations, such as those that rely on the classic Wiener approach, we have developed an algorithm for exploring random walks based on random temporal steps that are uniformly distributed in logarithmic time. This improvement enables us to generate random-walk trajectories of probe particles that span a highly extended dynamic range in time, thereby facilitating the exploration of probe motion in soft viscoelastic materials. By combining this faster approach with a Maxwell-Voigt model (MVM) of linear viscoelasticity, based on a slowly diffusing harmonically bound Brownian particle, we rapidly create trajectories of spherical probes in soft viscoelastic materials over more than 12 orders of magnitude in time. Appropriate windowing of these trajectories over different time intervals demonstrates that random walk for the MVM is neither self-similar nor self-affine, even if the viscoelastic material is isotropic. We extend this approach to spatially anisotropic viscoelastic materials, using binning to calculate the anisotropic mean square displacements and creep compliances along different orthogonal directions. The elimination of a fixed time step in simulations of random processes, including random walks, opens up interesting possibilities for modeling dynamics and response over a highly extended temporal dynamic range.

DOI: 10.1103/PhysRevE.89.042309 PACS number(s): 82.70.Dd, 05.40.Fb, 83.60.Bc, 66.30.hk

The classic random walk algorithm, which has a fixed time step, is a simple, yet powerful, simulation method for generating ensembles of self-similar trajectories that model important physical phenomena, such as Brownian motion of colloidal particles in an isotropic viscous medium. The basic method of generating a random walk was first introduced by Lord Rayleigh [1] in the context of sound wave propagation in heterogeneous media; a sequence of random wave vectors, each having a fixed amplitude but a random phase, was summed. Thus, this simple method considers a constant spatial step size that can be taken in random directions, with symmetric or weighted probability, and, at sufficiently long times, it can be used to predict the linear variation of the mean square displacement with time that is well known in diffusion. The Wiener process, while keeping a single fixed time step, introduced variable spatial step sizes, which typically have a normal (i.e., Gaussian) distribution, and this process has been highly successful in describing Brownian motion of a probe sphere in a simple isotropic viscous fluid [2]. The Gaussian random walk can be described as the sum of a series of independent but normally distributed random variables having a mean of zero. The standard deviation of the random variables sets an important system property: the diffusion coefficient.

In the simple limiting case of an isotropic viscous medium, the Brownian motion of a diffusing spherical probe is ergodic, and the step sizes for each degree of freedom are characterized by random numbers that are Gaussian distributed, where the mean is zero and the standard deviation (SD) depends on the diffusion coefficient D of the medium. For a two-dimensional (2D) isotropic medium, the individual mean squared displacements (MSDs) are given by: $\langle \Delta x^2(\tau)\rangle = \langle \Delta y^2(\tau)\rangle = 2D\tau$, where τ is the time lag, the diffusion coefficient according to the Stokes-Einstein relation is $D = k_B T/(6\pi\eta a)$, the sphere's radius is a, the medium's viscosity is η, and the temperature is T [3]. Consequently, the two-dimensional MSD, where the displacement vector is $\Delta \boldsymbol{r}$, is simply given by $\langle \Delta \boldsymbol{r}^2(\tau)\rangle = 4D\tau$. Here, the flows around the sphere are three dimensional and observations of its center position are made in 2D, as is common for most optical microscopy experiments.

Many variations of the classic random walk algorithm have been previously made [4]. These include adaptations for exploring a variety of fractal structures [5–7]; modeling a one-dimensional (1D) random walk on a chain in the presence of an attractive center [8]; sticking points in between constant velocity states [9]; diffusion-limited aggregation (DLA) behavior of metal particles [10,11]; slippery DLA of spheres that do not have rigid sticky bonds [12]; the Saffman-Taylor problem in fluid mechanics using DLA [13]; and anisotropic diffusion of cylindrical and disk-shaped particles for studying DLA of anisotropic shapes that introduced the idea of a "touch space" [14]. Both convective flows in the system and motion of self-propelled particles [15,16], such as trajectories of swimming micro-organisms [17], have also been simulated using a biased random walk. Moreover, to model active heterogeneous media, characteristic of living cytoplasm, a random walk code has been developed to simulate the diffusion and ballistic motion of a probe particle in a heterogeneous medium having spatial confinement sites [18].

Soft viscoelastic materials can have a spectrum of mechanical relaxation responses that covers many orders of magnitude in time. In thermal passive microrheology, solid spherical particles are often embedded at highly dilute concentrations as tracer probes into soft materials, and their thermally excited trajectories are observed and measured using 2D particle-tracking microscopy over a large dynamic range in time [19–21]. Subdiffusive and caged behaviors can be observed since the elasticity of these materials can be time, or equivalently, frequency dependent. Thus, because

*Corresponding author: mason@physics.ucla.edu

of their inherently complex responses that can span many decades in time, viscoelastic materials present a particular challenge for modeling using a classic random walk algorithm. Restricting attention to nonglassy, ergodic materials that have a long-time relaxation simplifies this general problem considerably. Even so, an idealized viscoelastic random walk algorithm must still preserve important physical principles, such as energy equipartition and the fluctuation-dissipation theorem.

Here, we construct a viscoelastic random walk algorithm that can be used to model Brownian motion of an isolated spherical particle in a model homogeneous viscoelastic material: a classic Voigt solid which also exhibits a Maxwell relaxation at long times. This basic Maxwell-Voigt model (MVM) captures the primary viscoelastic features of many kinds of soft materials, such as wormlike micelles [22], emulsions [23], and concentrated dispersions [23] using very few parameters [24–26]. Moreover, by contrast to classic random walk codes, which use a fixed time step, instead, we introduce a faster algorithm based on random time steps that are uniformly distributed in logarithmic time (UDLT) for creating trajectories which span highly extended dynamic ranges in time, more than 12 orders of magnitude. In addition, we generalize this approach to spatially anisotropic viscoelastic materials, motivated by shear-aligned micellar gels [27], liquid crystalline polymers [28], and soft tissue structures [29]. We demonstrate that distinguishing the anisotropy clearly can depend upon the observed range of time scales in experiments. We calculate 2D trajectories and determine 1D and 2D mean squared displacements (MSDs) of spherical probe particles in model MVM viscoelastic media.

By contrast to simple viscous liquids, in viscoelastic materials, the MSD does not exhibit a simple linear dependence on τ; instead, subdiffusive and plateau behaviors are typically observed [20,21]. Here, we consider viscoelastic materials that are ergodic and obey a MVM, which is a combination of the classic Maxwell and Voigt models [24,25,30], where the plateau elastic modulus G_p of both models is matched at intermediate frequencies. At very high frequencies $1/\tau$, the response is viscously dominated, whereas at very low frequencies, there is a slow viscous relaxation typically arising from thermal reorganization of colloidal structures in the viscoelastic material. The MVM, albeit idealized, captures the most basic features of many common viscoelastic soft materials. The Maxwell part of the MVM has a low-frequency viscosity η, and the characteristic low-frequency Maxwell relaxation time is $\lambda = \eta/G_\mathrm{p}$. The Voigt part has a matching G_p and also a high-frequency viscosity, η_s, typically associated with a solventlike viscous continuous phase; the characteristic high-frequency crossover time between elastic and viscous behavior is $\lambda_\mathrm{B} = \eta_\mathrm{s}/G_\mathrm{p}$. Probe-sphere motion in the MVM is equivalent to a harmonically bound Brownian particle (HBBP), which effectively captures the Voigt part, yet also includes the long-time diffusion of the bounding harmonic potential well with the same characteristic Maxwell relaxation time λ [23]. In the HBBP, the probe sphere performs Brownian motion in a medium having viscosity η_s, under the influence of a harmonic potential with elastic restoring force $-k\Delta x$, where the force constant is $k = 6\pi a G_\mathrm{p}$, assuming stick boundary conditions [20,21]. To include the Maxwell relaxation, we require that the center of this potential well must also perform Brownian motion for time scales significantly larger than λ.

Ignoring inertial effects, the Langevin equation for the forces along the x direction acting on a spherical particle, according to the simple HBBP, is given by

$$0 = F_\mathrm{r}(t) - kx - 6\pi a\eta_s \frac{dx}{dt}, \tag{1}$$

where $F_\mathrm{r}(t)$ is the Brownian random force, which has a white-noise frequency spectrum characterized by a delta-correlated temporal response: $\langle F_\mathrm{r}(t)\rangle = 0$ and $\langle F_\mathrm{r}(t)F_\mathrm{r}(t')\rangle = 12\pi a\eta_\mathrm{s}k_\mathrm{B}T\delta(t-t')$. By solving this Langevin equation, one obtains the Green's function, $G(x, x_0; t)$, which gives the probability of finding a particle at x after a time interval t for the initial condition $x = x_0$ at $t = 0$ [31,32]:

$$G(x,x_0;t) = [2\pi B(t)]^{-1/2}\exp\left\{-\frac{[x-A(t)]^2}{2B(t)}\right\}, \tag{2}$$

where

$$A(t) = x_0\exp(-t/\lambda_\mathrm{B}), \tag{3}$$

and

$$B(t) = \frac{k_\mathrm{B}T}{k}[1-\exp(-2t/\lambda_\mathrm{B})]. \tag{4}$$

Here, the time that the particle takes to reach equilibrium in the potential well is $\lambda_\mathrm{B} = 6\pi a\eta_\mathrm{s}/k$. The Green's function $G(x, x_0; t)$ is a Gaussian positional distribution centered around $A(t)$, which represents the ensemble-averaged position of the particle at time t, and having variance $B(t)$. For $t \gg \lambda_\mathrm{B}$, the Green's function reduces to the Boltzmann distribution and B ($=k_\mathrm{B}T/k$ in this limit) effectively reflects the saturated plateau value in the MSD corresponding to the harmonically bound motion. A similar equation of motion and solution can be written along the orthogonal $\hat{y}$ direction, neglecting any coupling between the directions mediated by the viscoelastic medium. We assume that the system size is infinite, so we have not applied any closed boundary condition.

To simulate the tracer bead trajectories in 2D, we generate two sets of Gaussian-distributed random numbers, each containing N elements, where N is the number of steps in the trajectory, using the polar algorithm in MATLAB. The first set, $R1_x$, corresponds to the x direction and the second set, $R1_y$, corresponds to the y direction. Each set has a mean of zero and a SD of unity. The time step size, Δt, is not constant; instead, it is a 1D array of N values: Δt_i, where i is an integer index. Thus, the total capture time of a trajectory can be given by $t_\mathrm{tot} = \sum_{i=1}^{N}\Delta t_i$. To form the Brownian motion of the harmonic well we create the step sizes, Δx_HW and Δy_HW, characterized by a set of Gaussian-distributed random numbers having zero mean and variance $2D_\mathrm{HW}\Delta t$, where $D_\mathrm{HW} = k_\mathrm{B}T/(6\pi\eta a)$ is the associated diffusion coefficient. Therefore, Δx_HW and Δy_HW can be generated from $R1_x$ and $R1_y$ by scaling the SD with $\sqrt{2D_\mathrm{HW}\Delta t}$. Since the time step size Δt in not constant, this needs to be done independently for each element, specifically by multiplying $R1_{x,i}$ and $R1_{y,i}$ with $\sqrt{2D_\mathrm{HW}\Delta t_i}$. The motion of the probe sphere according to the HBBP is simulated in the reference frame of the harmonic well. The positional time series of the center of the HBBP, $x_\mathrm{HBBP}(t)$ and $y_\mathrm{HBBP}(t)$, as defined by the Green's function, can be characterized by sets

of Gaussian-distributed random numbers having mean $A(t)$ and SD $= \sqrt{B(t)}$. For this, we generate two new sets of random numbers $R2_x$ and $R2_y$, following the same method and having same characteristics as that of $R1_x$ and $R1_y$. Each element of $R2_x$ and $R2_y$ is modified to construct the positional time series as $x_{\mathrm{HBBP},i} = (R2_{x,i}\sqrt{B_i} + A_{x,i})$ and $y_{\mathrm{HBBP},i} = (R2_{y,i}\sqrt{B_i} + A_{y,i})$. Knowing the system parameters and the initial position of the HBBP, $x_{\mathrm{HBBP},i-1}$ and $y_{\mathrm{HBBP},i-1}$, A_i and B_i are calculated corresponding to each time step Δt_i using Eqs. (3) and (4), respectively. Thus, the position of the harmonic well after the time step Δt_i is given by $x_{\mathrm{HW},i} = \sum_{n=1}^{i} \Delta x_{\mathrm{HW},n}$ and $y_{\mathrm{HW},i} = \sum_{n=1}^{i} \Delta y_{\mathrm{HW},n}$, and the positional time series of the HBBP in reference to the laboratory frame, $x_i = x_{\mathrm{HBBP},i} + x_{\mathrm{HW},i}$ and $y_i = y_{\mathrm{HBBP},i} + y_{\mathrm{HW},i}$, gives the tracer bead's trajectory.

We have also simulated trajectories for complex anisotropic viscoelastic systems in which the low-frequency viscosity and plateau elastic moduli have different values along orthogonal directions. The diffusion coefficients associated with the Brownian motion of the center of the harmonic well now can be defined as $D_{\mathrm{HW},x} = k_{\mathrm{B}}T/(6\pi\eta_x a)$ and $D_{\mathrm{HW},y} = k_{\mathrm{B}}T/(6\pi\eta_y a)$. Therefore $R1_x$ and $R1_y$ are treated separately with $\sqrt{2D_{\mathrm{HW},x}\Delta t_i}$ and $\sqrt{2D_{\mathrm{HW},y}\Delta t_i}$, respectively, to generate $\Delta x_{\mathrm{HW},i}$ and $\Delta y_{\mathrm{HW},i}$. The anisotropy in G_{p} is also reflected in the force constant k; in turn, $A(t)$ and $B(t)$ become anisotropic. Therefore, the positional time series of the HBBP is generated as $x_{\mathrm{HBBP},i} = R2_{x,i}\sqrt{B_{x,i}} + A_{x,i}$ and $y_{\mathrm{HBBP},i} = R2_{y,i}\sqrt{B_{y,i}} + A_{y,i}$.

Calculating the MSD from a trajectory generated by the UDLT algorithm by binning is straightforward. We first define M bins in τ that are logarithmically spaced, so M is the number of desired data points in the MSD plot. For each of $N(N-1)/2$ possible time lag values, $\tau_k = t_i - t_j$, where both i and j can take any values from 1 to N, the MSDs can be calculated as $\langle (x_i - x_j)^2 \rangle$ and $\langle (y_i - y_j)^2 \rangle$ in 1D and as $\langle (x_i - x_j)^2 + (y_i - y_j)^2 \rangle$ in 2D. All the τ_k values that belong to the mth bin, satisfying $m_{\mathrm{s}} < \tau_k < m_{\mathrm{e}}$, where m_{s} and m_{e} are the starting and ending times, respectively, of the mth bin, are averaged and then plotted versus the bin's geometric mean time, $(m_{\mathrm{s}}m_{\mathrm{e}})^{1/2}$.

To generate smooth MSD curves over a wide dynamic range of τ, we simulate trajectories having very long total times t_{tot} yet a very small shortest time step Δt. In a conventional random walker simulation that uses a fixed shortest time step, this would necessarily require a very large number of steps $N_{\mathrm{conv}} = t_{\mathrm{tot}}/\Delta t$. This, in turn, would demand a much larger number of calculations to generate the trajectory and calculate the MSD, at least with a scaling $\sim N_{\mathrm{conv}}^2$. Here, we have developed a faster route that covers many decades of τ with sufficient smoothness in the MSD, dramatically reducing the number of CPU operations. Instead of using constant Δt, our approach is to use a set of random Δt that are uniformly distributed in logarithmic time. The set of Δt_i, containing N elements, is generated as 10^{R3}, where $R3$ represents a set of uniformly distributed pseudorandom numbers in the open interval $\{\log_{10}(\Delta t_{\mathrm{min}}), \log_{10}(\Delta t_{\mathrm{max}})\}$, Δt_{min} is the smallest allowed time step, and Δt_{max} is the largest allowed time step. The number of decades in time is $N_{\mathrm{d}} = \log_{10}(\Delta t_{\mathrm{max}}/\Delta t_{\mathrm{min}})$. Consequently, at least some values in the set of Δt_i are very large and thereby contribute to the long τ regime in the MSD, yet at least some other values in the set of Δt_i are very small and thereby contribute to the short τ behavior. Although t_{tot} can differ from one trajectory to another under the UDLT approach, it can be estimated by $t_{\mathrm{tot}} \approx \Delta t_{\mathrm{max}}(N/N_{\mathrm{d}})$. Assuming Gaussian statistics, the ratio N/M effectively sets the smoothness of the MSD to a variation at or below $(M/N)^{1/2}$. Typically, three to five points per decade (i.e., $3 \leqslant M/N_{\mathrm{d}} \leqslant 5$) in the MSD are sufficient to capture interesting nondiffusive features, and this is certainly true for the MVM. Thus, N can be chosen depending on the desired variation in smoothness and number of points per decade.

We use the UDLT approach to produce 2D trajectories and MSDs having $t_{\mathrm{tot}} \approx 10^7$ s and $M = 36$ with $\Delta t_{\mathrm{min}} = 10^{-8}$ s and $\Delta t_{\mathrm{max}} = 10^4$ s, such that MSD curves having $M/N_{\mathrm{d}} \approx 3$ are smooth to at least about $(M/N)^{1/2} \approx 2\%$ variation over more than $N_{\mathrm{d}} = 12$ decades, using only $N = 150\,000$ steps $\ll \mathrm{N_{conv}} = 10^{12}$ steps. There are more than N/N_{d} (i.e., $\approx 12\,500$) elements in each set of Δt_i that belong to a temporal decade, ensuring sufficient averaging to generate smooth MSD curves up to lag times that are at least an order of magnitude less than t_{tot} but can be significantly larger than Δt_{max}. The number of CPU operations required for calculating the MSD using the logarithmic distribution approach increases $\sim N^2$, yet since $\mathrm{N} \ll \mathrm{N_{conv}}$, the UDLT approach is much faster than the conventional approach, which scales as $\sim N_{\mathrm{conv}}^2$. Exploiting the UDLT approach, the CPU time required for generating such a 12-decade trajectory and calculating its MSD is only a few hours on a 2.7 GHz Intel Core i7 processor.

We produce trajectories of a spherical probe particle and calculate corresponding MSDs in complex viscoelastic media for three different cases. In the first case, both the viscoelastic medium and the solvent have spatially isotropic properties, so particle trajectories, on average, exhibit no preferred direction. We next explore how spatial anisotropy in the viscoelastic properties, i.e., where G_{p} and η depend on direction, can affect the trajectories and MSDs. In a second case, both G_{p} and η have lower values along $\hat{x}$, compared to those along $\hat{y}$. In the third case, the plateau elasticity is lower along $\hat{x}$, $G_{\mathrm{p},x} < G_{\mathrm{p},y}$, whereas the long-time viscosity is lower along $\hat{y}$, $\eta_x > \eta_y$. In these anisotropic cases, the tracer bead trajectories show asymmetric spatial preference for particular directions that depend on the time scale of observation. In all herein simulations, the tracer bead diameter is taken as $2a = 2\ \mu$m, and the temperature is $T = 300$ K.

To demonstrate the time evolution of a typical tracer bead trajectory, as might be observed in a particle-tracking microrheology experiment using a fixed capture rate, five subtrajectories with increasing capture times, $t_{\mathrm{tot}} = 10^{-7}, 10^{-5}, 10^{-1}, 10^2$, and 10^3 s, are plotted for each of the three cases. The subtrajectories, generated with a constant time step $\Delta t = t_{\mathrm{tot}}/(5 \times 10^4)$, are representative examples of portions of the full UDLT trajectory that has been used to calculate the MSD. Since Δt is larger for the subtrajectories with longer t_{tot}, the step sizes are coarse-grained jumps from one position at t to another position at $t + \Delta t$ and those subtrajectories do not look like generic diffusive motion. To demonstrate the subtrajectories for $t_{\mathrm{tot}} = 10^2$ and 10^3 s with better clarity, the slower diffusive motion of the center point of the subtrajectory for $t_{\mathrm{tot}} = 10^{-1}$ s is superposed on the actual trajectories. From the isotropic MSD, we also calculate the 2D creep

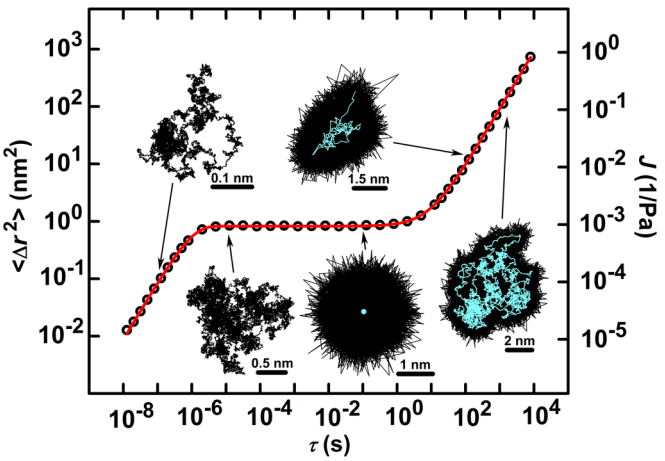

FIG. 1. (Color online) Time-averaged 2D MSD $\langle \Delta \boldsymbol{r}^2(\tau)\rangle$, creep compliance J, and subtrajectories over different ranges of observation times of a probe particle in a viscoelastic medium modeled by a Maxell-Voigt model (MVM) using a uniform random distribution in logarithmic time. Simulation results (open circles) fit well to a theoretical prediction, $4D\tau + r_0^2[1 - \exp(-\tau/\lambda_B)]$ (red line). Each subtrajectory is generated by 50 000 equidistant time steps and the capture times are 10^{-7}, 10^{-5}, 10^{-1}, 10^2, and 10^3 s (arrows) going from left to right. The scale bars denote the length scale associated with the subtrajectories. The slow diffusion of the center of the harmonic well is shown by the blue lines inside the subtrajectories.

compliance, $J(\tau)$, which is proportional to the MSD: $J(\tau) = 3\pi a\langle \Delta \boldsymbol{r}^2(\tau)\rangle/(2k_BT)$ [19]. Likewise, for anisotropic materials, along orthogonal 1D directions, we calculate $J_x(\tau) = 3\pi a\langle \Delta x^2(\tau)\rangle/(k_BT)$ and $J_y(\tau) = 3\pi a\langle \Delta y^2(\tau)\rangle/(k_BT)$. Together with the MSDs, we codisplay results for J, since it is proportional. For the anisotropic cases, the MSDs along the orthogonal directions are not identical and therefore the 1D MSDs along $\hat{x}$ and $\hat{y}$ are coplotted.

In Fig. 1, we present a few example subtrajectories of spherical probes, as well as the corresponding MSD and the creep compliance calculated from a full trajectory in 2D, $\langle \Delta r^2\rangle$, and J respectively, in an isotropic viscoelastic medium with $G_p = 10^3$ Pa and $\eta = 10^4$ Pa s dispersed in a solvent having $\eta_s = 10^{-3}$ Pa s (i.e., the viscosity of water). The effective ensemble-averaged area of a trajectory expands symmetrically for capture time $t_{tot} < 10^{-6}$ s, as shown by the trajectory from 10^{-7} to 10^{-5} s. A trajectory associated with the plateau region of the MSD does not expand with time; instead the particle remains bound in the harmonic well, as exhibited by the circular-shaped spatially restricted trajectory (e.g., as shown for $t_{tot} = 10^{-1}$ s). As the capture time t_{tot} for a trajectory increases and crosses the plateau region, the bound trajectory as a whole diffuses symmetrically and the area of the trajectory starts increasing again with t_{tot}. Trajectories corresponding to $t_{tot} = 10^2$ s and $t_{tot} = 10^3$ s display this behavior, where the superposed curve (light blue) shows the diffusive motion of the bound trajectory.

We fit the calculated 2D MSD for the isotropic MVM to an equation $\langle \Delta r^2\rangle = 4D\tau + r_0^2[1 - \exp(-\tau/\lambda_B)]$ corresponding to a HBBP that also exhibits long-time diffusion with $D = k_BT/(6\pi\eta a)$ associated with the Maxwell viscosity. The square of the saturated displacement in the plateau region is r_0^2, and the characteristic crossover time of the HBBP is λ_B. This equation can be obtained by inverse transformation of an ensemble-averaged Laplace-transformed solution to the Langevin equation in a manner that satisfies energy equipartition and the fluctuation-dissipation theorem, following steps similar to those given in Mason *et al.* [23]. In 2D, r_0^2 is related to G_p by $r_0^2 = 4k_BT/(6\pi a G_p)$. To validate the results of our simulations, we fit the calculated MSD in the isotropic MVM viscoelastic medium; the fitted (solid red) curve shows excellent agreement with the MSD calculated from our simulated trajectory. The three fit parameters D, r_0^2, and λ_B for only a single time-averaged trajectory all match to within better than 10% of the values we have selected for the simulation through η_s, G_p, and η, even without considering weighting the calculated MSD values, which span many decades and without ensemble averaging.

In the second case, we consider an anisotropic viscoelastic MVM material which has an elastic modulus and a long-time viscosity along $\hat{y}$ that are twice as large as along $\hat{x}$: $G_{p,x} = G_{p,y}/2 = 10^3$ Pa, $\eta_x = \eta_y/2 = 10^4$ Pa s. We assume that the short-time solvent viscosity is isotropic: $\eta_s = 10^{-3}$ Pa s. For this set of parameters, there is still only a single Maxwell relaxation time, irrespective of spatial direction. Figure 2 displays the 1D MSDs and creep compliances in spatial directions $\hat{x}$ and $\hat{y}$, along with a set of example trajectories for this case corresponding to different time ranges of observation. Both $\langle \Delta x^2\rangle$ and $\langle \Delta y^2\rangle$ exhibit behavior similar to $\langle \Delta r^2\rangle$ in Fig. 1, although both the height of the plateau and the diffusion coefficient for the linear rise at $\tau > 10$ s have larger values

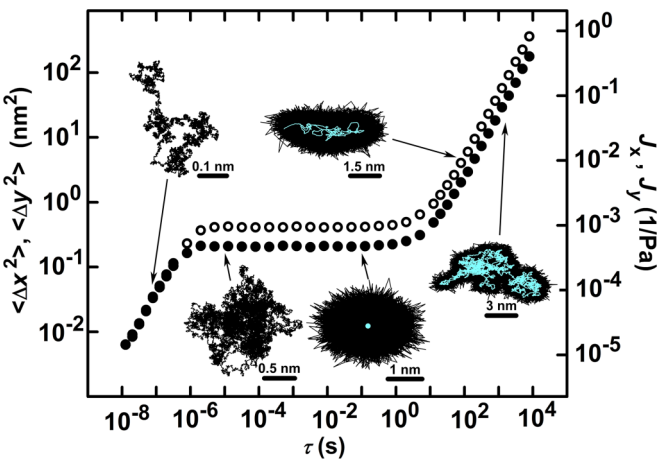

FIG. 2. (Color online) Time-averaged 1D MSDs $\langle \Delta x^2\rangle$ (open circles) and $\langle \Delta y^2\rangle$ (filled circles), corresponding creep compliances J_x and J_y, and 2D subtrajectories over different ranges of observation times of a spherical probe particle (1 μm radius) in an anisotropic MVM viscoelastic medium at temperature $T = 300$ K. The values of G_p and η along $\hat{y}$ are greater than those along $\hat{x}$ by a factor of 2; the solvent viscosity η_s is chosen to be isotropic. The subtrajectories having total capture times of 10^{-7}, 10^{-5}, 10^{-1}, 10^2, and 10^3 s are generated using 50 000 equidistant time steps for each case (arrows point to corresponding capture times). The scale bars show the length scales of the corresponding subtrajectories. The blue line within the subtrajectories shows the slow diffusive motion of the center of the harmonic well.

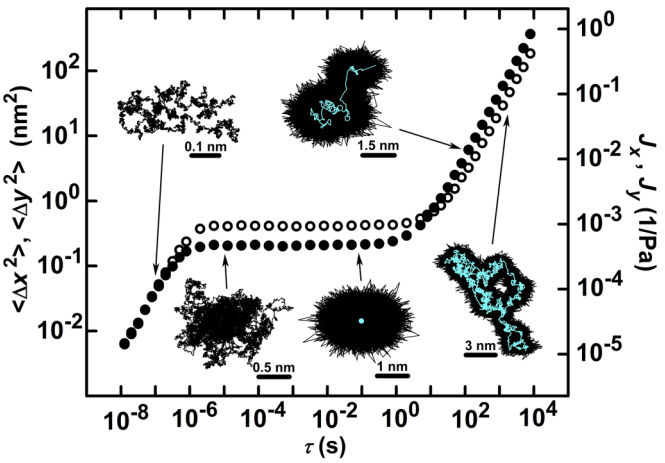

FIG. 3. (Color online) Time-averaged 1D MSDs $\langle \Delta x^2 \rangle$ (open circles) and $\langle \Delta y^2 \rangle$ (filled circles), corresponding creep compliances J_x and J_y, and 2D subtrajectories over different ranges of observation times of a probe particle in a viscoelastic medium having anisotropic Maxwell viscoelastic parameters along $\hat{x}$ and $\hat{y}$. Here, the value of G_p along $\hat{y}$ is greater than that along $\hat{x}$ by a factor of 2, and the long-time viscosity is less: $\eta_y = \eta_x/2$. The solvent viscosity η_s is chosen to be isotropic, so $\langle \Delta x^2 \rangle$ and $\langle \Delta y^2 \rangle$ overlap at short times. Subtrajectories are generated as described in Fig. 2 (caption).

for $\langle \Delta x^2 \rangle$ compared to those for $\langle \Delta y^2 \rangle$. The MSD plots at $\tau < 10^{-6}$ s overlap because the high-frequency viscosity is isotropic. Considering an ensemble of generated trajectories, on average, trajectories grow symmetrically with capture time t_{tot} up to $t_{tot} < 10^{-6}$ s. However, for larger 10^{-6} s $< t_{tot} <$ 10^0 s, the saturated square displacements associated with the plateau region in the MSDs are different along the orthogonal directions, and hence, the spatially restricted trajectory takes an elliptical shape where the long axis is oriented along $\hat{x}$. For $t_{tot} > 10$ s, the elliptical bound trajectory also diffuses asymmetrically, preferentially along $\hat{x}$ (see blue interior lines), and this trend continues into the viscous relaxation regime at very long times.

For a third case, we generate a trajectory that can appear to be more elongated along different directions, depending on the time scales of observation. In Fig. 3, we show subtrajectories of a single trajectory, sampled at different observation times, and calculated 1D MSDs $\langle \Delta x^2(\tau) \rangle$ and $\langle \Delta y^2(\tau) \rangle$, along with corresponding $J_x(\tau)$ and $J_y(\tau)$, for the following anisotropic viscoelastic parameters: $G_{p,x} = G_{p,y}/2 = 10^3$ Pa, $\eta_x/2 = \eta_y = 10^4$ Pa s, and an isotropic solvent viscosity $\eta_s = 10^{-3}$ Pa s. The slow Maxwell relaxation time along $\hat{x}$ is $\lambda_x = \eta_x/G_{p,x} = 20$ s, four times greater than $\lambda_y = \eta_y/G_{p,y} = 5$ s along $\hat{y}$. For the shortest times, the subtrajectories first expand symetrically with t_{tot}, as demonstrated by the trajectory for $t_{tot} = 10^{-7}$ s and $t_{tot} = 10^{-5}$ s. In the plateau region, the subtrajectories get restricted in space with an asymmetric shape elongated along $\hat{x}$. However, at very long times for $t_{tot} > 10$ s, the subtrajectories become elongated in the opposite direction, along $\hat{y}$. Thus, for this type of anisotropic viscoelastic material, the overall elongation in the trajectories changes direction if the observation times are limited to a smaller range, corresponding to the subtrajectories.

The trajectories that we have generated provide a view of Brownian random walks in viscoelastic media over a much greater dynamic range than any prior experimental particle-tracking microrheology studies. We anticipate that having an alternative numerical method of rapidly generating such trajectories and MSDs over many decades in time will aid in the interpretation of particle-tracking microrheology experiments covering a wide range of isotropic and anisotropic viscoelastic media. For an isotropic system, the ensemble-averaged trajectories are symmetric in shape irrespective of the observation time.

In the more complex anisotropic MVM systems, the viscoelastic parameters can have different values along two orthogonal directions, and the ensemble-averaged trajectories can have different asymmetries in their shapes depending upon the range of observation times. In the elastic plateau region, for anisotropic elastic media, the bound trajectories take on an elliptical shape, having larger saturated displacement, and hence, lower plateau elastic modulus, along a particular direction that could arise from an anisotropic internal colloidal structure of the medium. Thus, experimental trajectories would be easier to analyze if the data are transformed so that one of the Cartesian axes is aligned along the long axis of the ellipse, yet identifying the principal axes could be challenging. Anisotropic systems can have different relaxation times along different directions, which may or may not be simply orthogonal. If the axes of anisotropy are orthogonal, a first step in analyzing probe particle trajectories in anisotropic viscoelastic media would be to determine the orientation of these axes relative to the laboratory frame. In the plateau region, where the particle performs a confined random walk, the time-averaged shapes of the trajectories (as well as the motion of the center of the harmonic well) make it relatively simple to detect the principal axes defining the anisotropy. However, in viscously dominated regimes, either at short or at long times, one trajectory may not be sufficient to point out the preferential relaxation direction in most cases if the anisotropy is not extreme. Depending on how rapidly the medium relaxes at long times, an ensemble average of at least a few trajectories (e.g., five trajectories for the systems discussed here as examples) is needed to determine the principal axes with reasonable certainty. The smaller the anisotropy in the viscoelastic parameters, the more one needs to ensemble average many trajectories to detect the anisotropic viscoelastic behavior from calculated differences in the values of the microscopic parameters.

The viscoelastic response of soft materials, whether isotropic or not, can cause the random walk trajectories to have different appearances, depending on the time window of observation and the time scales associated with dominantly elastic and dominantly viscous responses. Thus, in general, random walks in isotropic viscoelastic media, such as what we have shown using the MVM, are *not self-similar* over all time scales, whereas they are in classic Brownian motion of an isolated sphere in a simple viscous liquid. Whereas a trajectory of a probe sphere in an anisotropic material that has a simple anisotropic viscosity over all time scales can be self-affine, for anisotropic viscoelastic media, this does not have to be

the case, since differences in the values of the plateau elastic moduli and the Maxwell relaxation times can destroy even the self-affine quality.

We anticipate that using the UDLT algorithm to reduce computational overhead will be advantageous when simulating and studying other soft viscoelastic systems that require a highly extended dynamic range in observation time. The UDLT random walk algorithm requires less time to generate trajectories and MSDs compared to calculating these piecewise from sets of short subtrajectories that can be stitched together to create a complete MSD plot. Because the UDLT algorithm is amenable to parallel processing, we expect that parallel UDLT codes will have even greater speed and economy than the non-parallel version implemented and described herein. Whether parallel or not, the speed increase in trajectory generation and analysis can be readily extended to multiparticle simulations. The initial modeling of viscoelasticity, which is based on a relatively simple MVM model, sets the stage for simulations of more complex spring-dashpot models of viscoelasticity. Moreover, the 2D simulation code can be easily extended to generate and study particle trajectories in 3D, including systems that have 3D anisotropic viscoelasticity. Treating and optimizing the inverse problem of finding principal axes and extracting anisotropic microrheological parameters from real anisotropic viscoelastic systems remains an interesting future direction. Performing such analysis on simulated trajectories will enable the establishment of quantitative bounds on the certainty of different microrheological viscoelastic parameters given limited experimental sampling.

By using random temporal step sizes that are uniformly distributed in logarithmic time, rather than only a single fixed time step, we have extended random walker simulations to cover an extremely large dynamic range while significantly reducing computational overhead. This UDLT algorithm, when combined with the anisotropic MVM, generates trajectories and MSDs of probe spheres in a model soft viscoelastic material over a highly extended dynamic range in time very rapidly. We have exploited this combination to study three different cases of a 2D MVM model: an isotropic case and also two anisotropic cases, including one that has different Maxwell relaxation times along each of the orthogonal directions. The trajectories that are produced are interesting and complex; because they are not self-similar at all times as a consequence of the elasticity, they are best displayed by windowing in sets of different time intervals. Thus, an anisotropic elasticity in a plateau region that persists over several decades can be unambiguously determined by time averaging a single trajectory, whereas at least a limited amount of ensemble averaging is required to distinguish anisotropic viscosities over a similar temporal range. We anticipate that this approach will be further extended into multiparticle simulations of trajectories of probe spheres in real viscoelastic materials in three dimensions.

[1] Rayleigh, Nature **72**, 318 (1905).
[2] W. Feller, Ann. Math. Stat. **22**, 427 (1951).
[3] A. Einstein, R. Furth, and A. D. Cowper, *Investigations on the Theory of the Brownian Movement* (Methuen & Co. Ltd., London, 1926).
[4] G. H. Weiss, *Aspects and Applications of the Random Walk* (North-Holland, New York, 1994).
[5] B. B. Mandelbrot, Phys. Scr. **32**, 257 (1985).
[6] Y. Shi and C. Gong, J. Phys. A **26**, L685 (1993).
[7] E. Bacry, J. Delour, and J. F. Muzy, Phys. Rev. E **64**, 026103 (2001).
[8] C. Aslangul, N. Pottier, P. Chvosta, D. Saint-James, and L. Skala, J. Stat. Phys. **69**, 17 (1992).
[9] E. R. Weeks and H. L. Swinney, Phys. Rev. E **57**, 4915 (1998).
[10] M. Y. Lin, H. M. Lindsay, D. A. Weitz, R. Klein, R. C. Ball, and P. Meakin, J. Phys.: Condens. Matter **2**, 3093 (1990).
[11] T. A. Witten, Jr. and L. M. Sander, Phys. Rev. Lett. **47**, 1400 (1981).
[12] C. R. Seager and T. G. Mason, Phys. Rev. E **75**, 011406 (2007).
[13] C. Tang, Phys. Rev. A **31**, 1977 (1985).
[14] J. R. Rothenbuhler, J. R. Huang, B. A. DiDonna, A. J. Levine, and T. G. Mason, Soft Matter **5**, 3639 (2009).
[15] A. F. Ghoniem and F. S. Sherman, J. Comput. Phys. **61**, 1 (1985).
[16] J. P. Bouchaud, A. Georges, J. Koplik, A. Provata, and S. Redner, Phys. Rev. Lett. **64**, 2503 (1990).
[17] N. A. Hill and D. P. Hader, J. Theor. Biol. **186**, 503 (1997).
[18] D. Weihs, M. A. Teitell, and T. G. Mason, Microfluid. Nanofluid. **3**, 227 (2007).
[19] T. M. Squires and T. G. Mason, Annu. Rev. Fluid Mech. **42**, 413 (2010).
[20] T. G. Mason and D. A. Weitz, Phys. Rev. Lett. **74**, 1250 (1995).
[21] T. G. Mason, H. Gang, and D. A. Weitz, J. Mol. Struct. **383**, 81 (1996).
[22] N. Willenbacher, C. Oelschlaeger, M. Schopferer, P. Fischer, F. Cardinaux, and F. Scheffold, Phys. Rev. Lett. **99**, 068302 (2007).
[23] T. G. Mason, H. Gang, and D. A. Weitz, J. Opt. Soc. Am. A **14**, 139 (1997).
[24] J. D. Ferry, *Viscoelastic Properties of Polymers* (Wiley, New York, 1970).
[25] R. B. Bird, R. C. Armstrong, and O. Hassager, *Dynamics of Polymeric Liquids* (Wiley, New York, 1987), Vol. 1.
[26] R. G. Larson, *The Structure and Rheology of Complex Fluids* (Oxford University Press, New York, 1999).
[27] M. Khan and A. K. Sood, Europhys. Lett. **92**, 48001 (2010).
[28] V. S. Volkov and V. G. Kulichikhin, J. Rheol. **34**, 281 (1990).
[29] J. E. Bischoff, E. M. Arruda, and K. Grosh, Biomech. Model. Mechanobiol. **3**, 56 (2004).
[30] B. R. Seymour and E. Varley, Proc. R. Soc. London, Ser. A **314**, 387 (1970).
[31] S. Chandrasekhar, Rev. Mod. Phys. **15**, 1 (1943).
[32] M. Doi and S. F. Edwards, *The Theory of Polymer Dynamics* (Oxford University Press, New York, 1986).